Reviews in Plasmonics

Chris D. Geddes *Editor*

Reviews in Plasmonics 2015

Springer

Reviews in Plasmonics

More information about this series at http://www.springer.com/series/7164

Chris D. Geddes
Editor

Reviews in Plasmonics 2015

Springer

Editor
Chris D. Geddes
Institute of Fluorescence
University of Maryland Baltimore County
Baltimore, MD, USA

ISSN 1555-7677
Reviews in Plasmonics
ISBN 978-3-319-24604-8 ISBN 978-3-319-24606-2 (eBook)
DOI 10.1007/978-3-319-24606-2

Library of Congress Control Number: 2015961024

Springer Cham Heidelberg New York Dordrecht London

Printed on acid-free paper

Springer International Publishing AG Switzerland is part of Springer Science+Business Media (www.springer.com)

Preface

This is the second volume in the Plasmonics series, *Reviews in Plasmonics*. The first volume was very well received by the Plasmonics community with several notable reviews of the volume.

In this 2015 volume, we are pleased again with the broad and timely Plasmonic content. We subsequently thank the authors for their very timely and exciting contributions again this year. We hope you all will find this volume as useful as the first volume.

In closing, I would like to thank both Tanja Koppejan and Meran Owen at Springer for their help in compiling this volume.

Institute of Fluorescence
University of Maryland Baltimore County
Baltimore, MD, USA
July 29 2015

Chris D. Geddes

Contents

Chapter 1
Surface Plasmon Polariton Assisted Optical Switching in Noble Metal Nanoparticle Systems: A Sub-Band Gap Approach

Sandip Dhara

Abstract Understanding the light-matter interaction at nanometre scale is a fundamental issue in optoelectronics and nanophotonics which are prerequisites for advanced sensor applications of optical switching. The electrical transport process in noble metal-insulator nanocomposite or dispersed noble metal nanocluster in dielectric matrix is discussed. Banking on high value of third-order nonlinear susceptibility, optical switching was reported in the percolation threshold of noble metals in dielectric matrices. The optical switching originating from the excitation of the surface plasmon was recorded for metal–oxide–metal tunnelling junctions. The surface plasma polariton (SPP) in the form of drifting hot electrons across the oxide barrier and tunnelling to the counter electrode in the evanescent field of surface plasmon resonance (SPR) was made responsible for electrical transport mechanism. These models, for the first time, are discussed in ambit of having a sub-band gap feature in the SPP assisted photoresponse where transport of electrical carriers may manifest either at the percolation threshold with enhanced electro-magnetic field, and in the form of tunnelling current through the potential barrier at the Fermi level or in the propagation of plasmon coupled electrons at SPR for metal-dielectric composites.

Keywords SPP • SPR • Optical switching • Noble metal • Nanoparticle

1.1 Introduction

Understanding the light-matter interaction at nanometre scale is a fundamental issue in optoelectronics and nanophotonics which are prerequisites for advanced sensor applications, namely, optical switching (abrupt change in resistance with exposed light signal) devises using all-optical signal processing [1, 2], two photon absorption (TPA) enhanced second harmonic generation (SHG) [3], renewable

S. Dhara (✉)
Surface and Nanoscience Division, Materials Science Group, Indira Gandhi Centre for Atomic Research, Kalpakkam 603 102, India
e-mail: dhara@igcar.gov.in

C.D. Geddes (ed.), *Reviews in Plasmonics 2015*,
DOI 10.1007/978-3-319-24606-2_1

energy resourcing by guiding and localizing light and considerable reduction in absorption layer thickness [4]. It is also used in the bio-organic sensing, in medical therapy encompassing early detection of beginning of life using shift in plasmonic resonance frequency due to the presence of molecular motors [5] and in destroying tumour by generating heat using the adiabatic heating of plasmonic vibration [6].

Optical switching using the enhanced third-order nonlinear susceptibility in noble metal systems [7–10], especially near the surface-plasmon-resonance (SPR) frequency evoked considerable interest among scientific researchers during last one and half decade. Coherent oscillation of conduction electrons, particularly in noble metal nanoclusters, with the excitation of visible light gives rise to surface plasmon polaritons (SPP) which propagate near the metal-dielectric interface (schematically shown in Fig. 1.1) [11–14]. The evanescent field allows the observation of interference [15–17], and sub-diffraction limited optical imaging of nanostructure [18–22]. The plasmon coupling within arrays of metal nanoparticles can lead to the formation of nanoscale hot spots in which the intensity of light from an incident beam can be concentrated by more than four orders of magnitude. The effect of light concentration by means of plasmon is most obvious in phenomena dealing nonlinearity in light intensity, as demonstrated recently by the on-chip generation of extreme-ultraviolet light by pulsed laser high harmonic generation [23]. This opens an affluence of prospects in lithography or imaging at the nanoscale through the use of soft x-rays. In fact, SPR induced localized SHG using Au nanoparticles are well studied system [24–26]. Among many such significant phenomena and applications, the most well known is the giant surface-enhanced Raman scattering (SERS) [27] or noble metal coated tip enhanced Raman scattering (TERS) [28], those allow both detection and spectroscopic imaging of a single molecule [29]. Electromagnetic energy transfer in chains of closely spaced metal nanoparticles was reported in the sub-diffraction limit by means of coupled plasmon modes [30, 31]. In a dispersion model for coupled plasmon modes considering equi-spaced metal nanoclusters is developed using an analytical

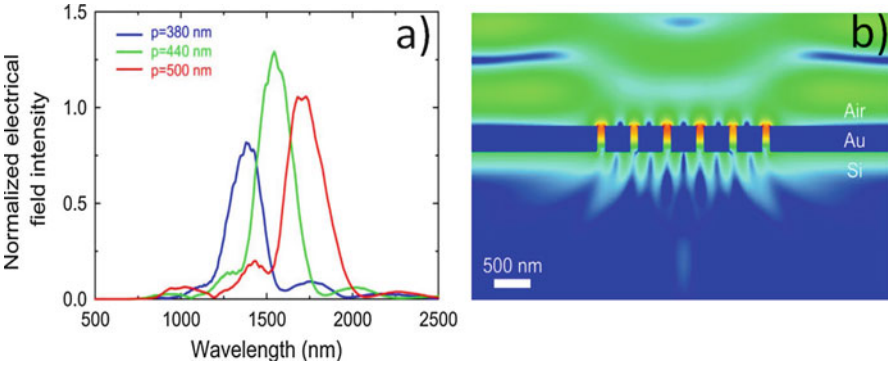

Fig. 1.1 (**a**) Incident-light wavelength dependencies of the electrical field intensity for different slit periods and (**b**) electrical field intensity distribution in a nano-slit grating for 1500 nm excitation (Ref. [14]; Copyright (2013) by the IEEE)

model that describes the near-field electromagnetic interaction between the particles in the dipole limit [30]. Coherent propagation with group velocities exceeding 0.1 c was calculated in straight wires of dimension less than 0.1λ (wavelength) and around sharp corners with bending radius less than wavelength of visible light. In another report using generalized Mie theory, the light-transport properties of Ag particles of 50-nm diameter, an optimum guiding conditions for an inter-particle spacing of 25 nm, and a corresponding 1/e signal-damping length of 900 nm was estimated [31]. These models of optical energy transport in a plasmonic chain are useful for sub-wavelength transmission lines within integrated optical circuits and for near-field optical microscopy in futuristic ultra fast photonic device applications.

Coinage elements of Au, Ag, Cu are extensively studied for plasmonic applications [32]. Ultrafast switching of 360 fs in Ag nanoclusters embedded in SiO_2 matrix, originating from self-diffraction of a pump pulse due to transient grating, was recorded in a femtosecond optical-Kerr-shutter experiment [7]. A very high optical nonlinearlity $\chi^{(3)} \sim 10^{-7}$ esu which was comparable [8] or one order lower [9] than that for Au nanoclusters system, was reported for Ag nanoclusters. An order lower value of $\chi^{(3)} \sim 10^{-8}$ esu was recorded on Cu nanoclusters dispersed in silica matrix with picosecond nonlinear optical response [10]. In a microreactor approach [33], Au NPs embedded in silica matrix showed optical switching with the exposure of 532 nm, which was close to the SPR absorption peak for Au NPs. In the similar approach, an optical switching was also reported for Au functionalized GaN (Au–GaN) nanowires with an excitation of 532 nm [34]. Role of band conduction in GaN is ruled out in the absence of optical switching using 325 nm (~3.8 eV) excitation (energy being higher than the band gap of GaN ~ 3.4 eV). The SPR, on the other hand, in bimetallic nanocluster of noble metals of Au and Ag is also useful for various applications with the ability of tuning the absorption peak position [35–37]. The SHG in the Pt/Cu [38] and Ag/Cu [39] systems drew lot of attention. In a recent report photoresponse of bimetallic Au–Ag nanoparticle embedded soda glass (Au–Ag@SG) substrate was reported [40] for surface plasmon assisted optical switching using 808 nm excitation, which was away from the characteristic SPR peaks of Ag (~400 nm) and Au (~550 nm) nanoparticles. The observation suggested the possible role of TPA owing to the presence of interacting electric dipole in these systems.

In order to understand the electrical transport process in noble metal-insulator nanocomposite or dispersed noble metal nanocluster in dielectric matrix, various models are discussed in the literature. Banking on high $\chi^{(3)}$ values, optical switching was reported in the percolation threshold of Au nanoclusters in SiO_2 matrix [9], and Cu nanoclusters on Si_3N_4 film [41]. A reversible electronic threshold switching was reported in percolative Ag nanoclusters embedded in polymer matrix [42]. The optical switching originating from the excitation of the surface plasmon was recorded for metal–oxide–metal tunnelling junctions [43]. The SPP in the form of drifting hot electrons across the oxide barrier and tunnelling to the counter electrode in the evanescent field of SPR was made responsible for electrical transport mechanism. In the specially designed experiment [34], optical switching

in Au–GaN nanowires with a sub-band gap excitation of 532 nm suggested possible role of SPP assisted transport of electron in the system. The same mechanism was proposed for the propagation of electronic carrier belonging to the conduction electron of noble bimetals in the Au–Ag@SG system in understanding the observed photoresponse [40]. Contributions of interband and intraband transitions in noble metals and inter-particle separation were discussed in understanding the plasmonic coupling mechanism. These models, for the first time, are discussed in ambit of having a sub-band gap feature in the SPP assisted photoresponse where transport of electrical carriers may manifest either at the percolation threshold with enhanced electro-magnetic field, and in the form of tunnelling current through the potential barrier at the Fermi level or in the propagation of plasmon coupled electrons at SPR for metal-dielectric composites.

1.1.1 A Percolative Pathway for Electrical Transport

Optical absorption and electrical transport properties of noble metal-dielectric nanocomposites can be understood from the theoretical investigation in the calculation of the dielectric function for a heterogeneous composite medium [44–46]. The Maxwell-Garnett theory (MGT), dealing predictions related to the existence of the optical dielectric anomaly observed in granular metal films (presently understood as absorption peak due to SPR of the noble metal clusters), was modeled for the calculation of optical properties [44]. However, MGT was limited in predicting observed percolation threshold in granular metals for the volume fraction of the metallic phase comparable to that of the matrix phase. On the other hand, the effective medium theory (EMT) was used for the calculation of the dielectric constant for composites, as well as predicted a percolation threshold for electrical conductivity [45]. However, unlike the MGT, dielectric anomaly could not be inferred in the EMT. Moreover, the predicted value of the percolation threshold was lower than that compared with the experimental reports. Later, based on a phenomenological model considering distribution of conducting and insulating phases, both the optical dielectric anomaly and the percolation threshold was developed for the unified understanding of the optical absorption and percolation transport properties of granular composite media [46]. At a specific composition with the fraction of conducting phase $p > 0.35$, a percolative pathway for electrical conduction was correctly estimated for Au–SiO_2 composite (Fig. 1.2). At the same time, as observed in experiments for the SPR absorption of Au clusters embedded in dielectric matrices was well described under the same formalism in the limit of the percolative compositions $0.1 < p < 0.8$ (Fig. 1.3). The percolating threshold was not predictable under MGT with optical anomaly existing even for $p = 1$. Transition in infrared transmission for $p > 0.7$ was another success of the model where also MGT failed to estimate. Subsequently, a hopping model in a percolative pathway, based on the microstructure of composites, was developed where the effect of charging energy E_c as a function of the conductance of paths linking grains of separation 's'

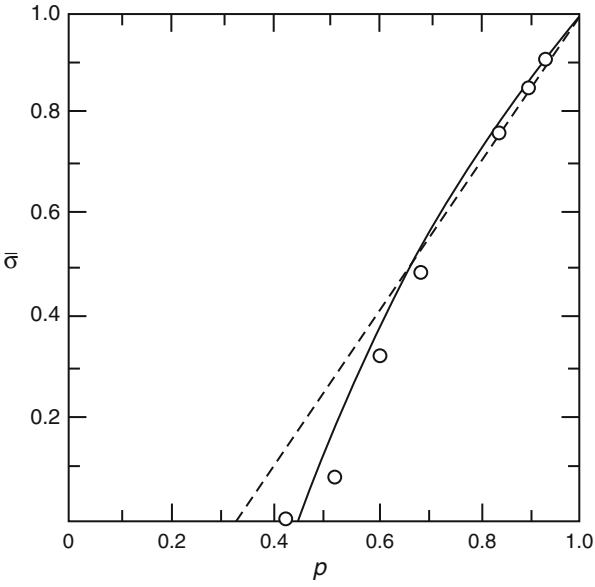

Fig. 1.2 Normalized conductivity $\bar{\sigma}$ as a function of p for Au–SiO_2 cermets. Data from Ref. [43]. *Dashed line* denotes EMT result (Ref. [46]; Copyright (1980) by the American Physical Society)

and diameter 'd' were considered with the assumption of constant s/d throughout the specimen [47]. Deviating from the phenomenological description, a band model was proposed in the percolating clusters [48], independent of microstructure, for estimating the activation energy from the intra-grain energy level splitting due to the finite size of the grains, apart from the usual electrostatic charging energy, E_c. Later on drawing an analogy with Efros-Shklovskii model [49], the role of 'site energy' was conceptualized in introducing correlated Coulomb gap [50]. A detailed study on electrical conductivity in the Ag nanoparticle embedded in glass matrix reported inter-grain hopping of charge carrier [51]. The characteristic temperature of the conductivity, $T_0 = 4\chi s E_c/k_B$, where k_B is the Boltzmann's constant and $\chi = (2m^*\varphi)^{1/2}/\hbar$ is the effective inverse tunneling width. Here, m^* is the effective mass of the charge carrier, and φ is the energy barrier over which the charge must hop, $\hbar$ is the reduced Planck's constant. The expression for $E_c = 2q^2 s/[\kappa d^2(½ + s/d)]$, where κ is the permittivity of the insulating phase and q is the electronic charge. The values T_0 was obtained from the slope of the temperature-dependent resistivity plot (Fig. 1.4a). In the scope of the sub-band gap hopping model, the trend in inter-particle separation with increased density of metallic phase, as estimated from the SPR peak analysis (Fig. 1.4b), was correctly calculated from the expression of T_0 and E_c with $\varphi \sim 4$ eV for glass matrix and d, the average size of the Ag clusters ~10 nm. Thus the role of sub-band gap states in the percolating noble metal clusters embedded in the dielectric matrices can be understood for the electrical transport in achieving optical switching.

Electrical conductivity at a threshold noble metal composition, $p > 0.6$ of percolative Au–SiO_2 composite was reported to increase abruptly along with a

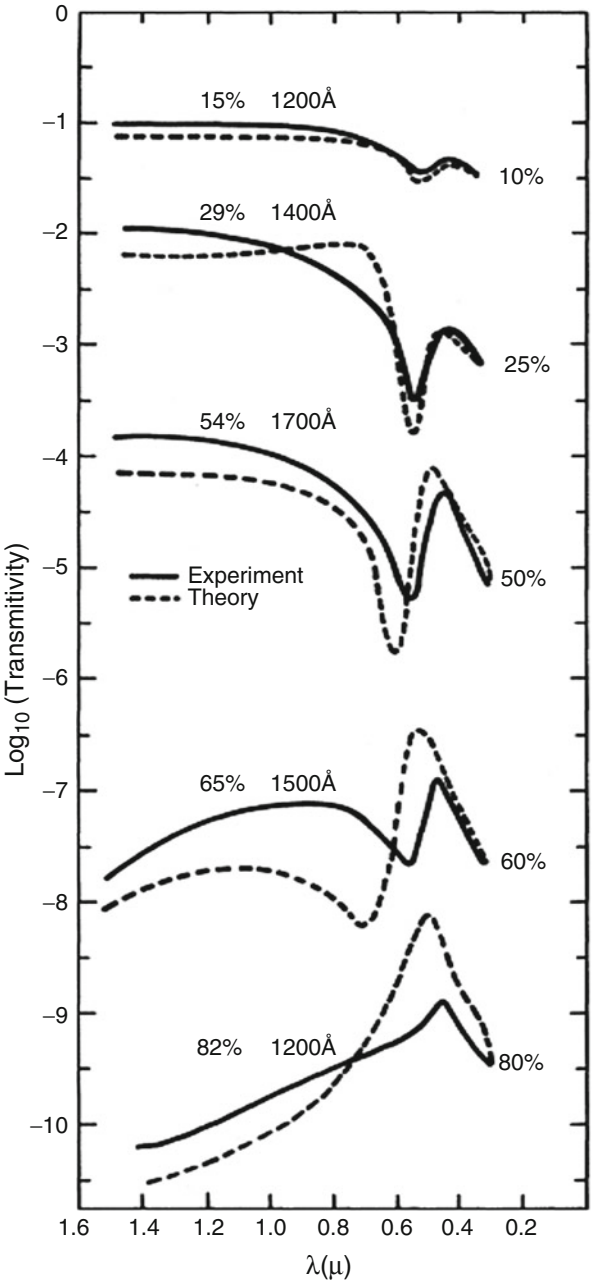

Fig. 1.3 Optical transmission as a function of light wavelength for a series of Au–SiO_2 composites. Data are from Ref. [43]. For clarity, the curves are displaced with respect to one another. The theoretical curves are normalized to the experimental values at 0.3 μm. The theoretical values of p are labelled to the right of pairs of curves, whereas the experimental values of p and the film thickness are given above each pair of curves (Ref. [46]; Copyright (1980) by the American Physical Society)

distinct change in the absorption pattern with infrared transmission increasing above the same threshold value. A collective effect of local field enhancement of the Au nanoclusters in combination with the increased light amplitude in resonant cavities formed between the surfaces of the optimally dense Au clusters embedded

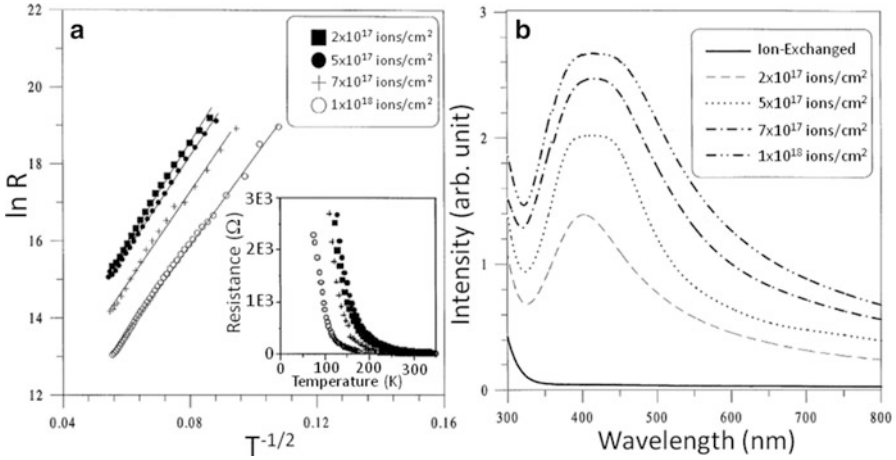

Fig. 1.4 (**a**) Plot of ln R versus $T^{-½}$ plot at various fluences. The inset shows resistance (R) versus temperature (T) plot. (**b**) Optical absorption spectra of ion exchanged and irradiated samples at various fluences (Ref. [51]; Copyright (2001) by the Elsevier Science B.V.)

in the SiO_2 matrix in the percolation limit was made responsible for the experimental observations [9]. In a unique study, light induced electrical conduction was reported in randomly-distributed Cu nanoparticles with varying surface coverage on an optically transparent Si_3N_4 [40]. At a percolation threshold of 64 % metal coverage, an optical switching was recorded corresponding to the peak wavelengths of the peak SPR (Fig. 1.5). Finite difference time domain (FDTD) simulation of the dielectric constants based on Drude-Lorentz-Sommerfeld model [52] in case of the Cu nanoparticles/Si_3N_4 system showed (Fig. 1.6) field enhancement at the percolation threshold. Thus, the report demonstrates that Cu nanoparticle-embedded device can detect the SPR by simply monitoring the current. The value of $\chi^{(3)}$ was found to depend on noble metal content in Ag:BiO_2 [53] and Cu:Al_2O_3 [54] composites with highest values achieved at the percolation threshold. The strong $\chi^{(3)}$ is responsible for optical switching in metal composite systems.

1.1.2 A Tunnelling Route to Electrical Transport

A reversible electronic switching effect was observed in Ag nanoparticles embedded in polymer films. A sharp change of up to six orders of magnitude in the current–voltage behavior are highly reversible for these nanocomposite materials, and are defined as threshold switching at a percolation threshold, 0.78 of the metallic coverage (Fig. 1.7) [42]. At the percolation threshold microstructure is characterized by near continuous chain of particles, with no conductive metallic path formed between the electrodes. At a specific gap of 2 nm or less between the particles, electric field of ~ 10^7 V/cm was estimated in between the Ag particles for

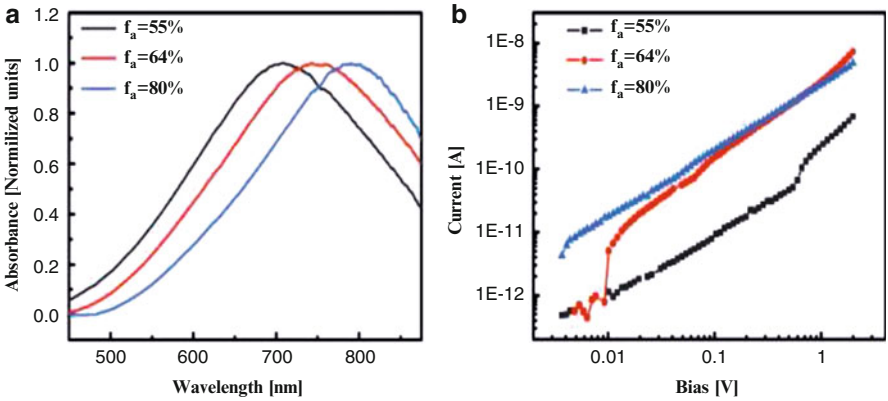

Fig. 1.5 (**a**) LSPR measurement results from samples with a surface coverage, f_a of 55 %, 64 %, and 80 %; each samples has a different resonance peak (55 %: 706 nm; 64 %: 743 nm; 80 %: 789 nm). (**b**) I–V characteristics of samples with a surface coverage of 55 %, 64 %, and 80 %; the plot of $f_a = 64$ % shows a jump of about one order of magnitude (for the percolation threshold) (Ref. [41]@2010, Copyright ©American Optical Society)

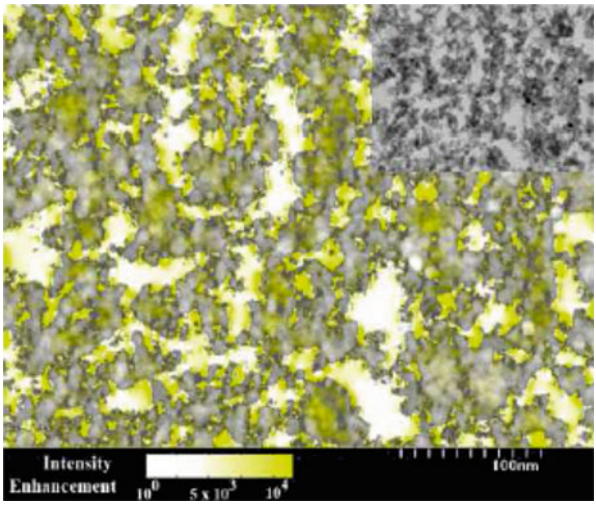

Fig. 1.6 Calculated electric field intensity enhancement in the plane of the deposited nanoparticles (64 % coverage sample). The local field intensity enhancement is depicted in the TEM image (inset) using the linear color bar (Ref. [41] @2010, Copyright©American Optical Society)

an applied voltage of 1 V between electrodes. A tunneling of electronic charges with relatively high current densities would occur through the potential barrier at the Fermi level in the field emission process at such a high field.

Narrow band photoresponsivities up to 60 mV /W into a l00 Ω impedance at 632.8 nm was observed in Ag–Al_2O_3–Al and Al–Al_2O_3–Al metal-insulator oxide-metal (MOM) devices [43]. The wavelength sensitivity of the detector could easily be varied over a wide range by coating the top electrode with different dielectrics, the upper limit being the SPP frequency of the top electrode. Optimum metal

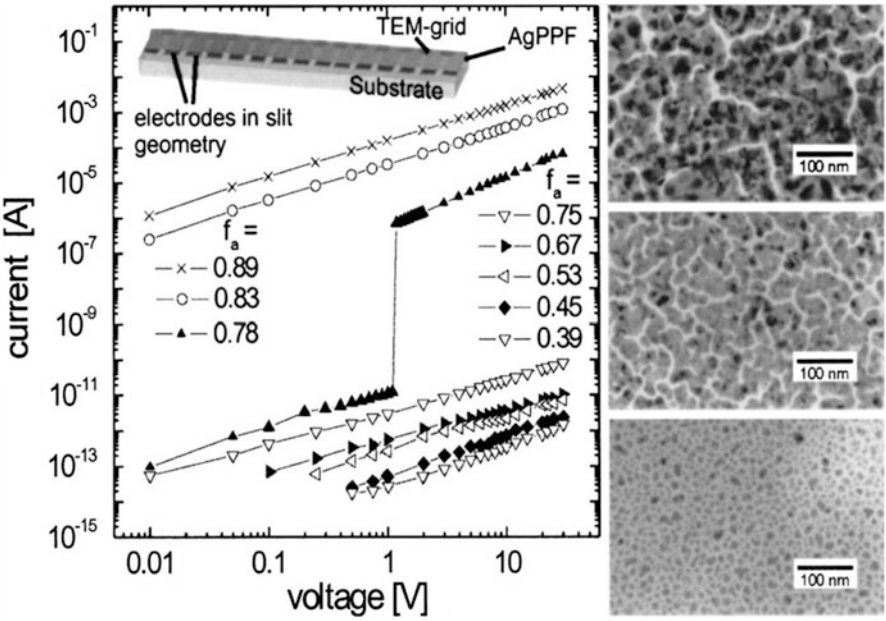

Fig. 1.7 *Left*: *I–V* characteristics of a plasma polymer film containing Ag nanoparticles (AgPPF) with different area filling factors f_a . *Top left*: Sample setup: Coplanar electrode arrangement (slit dimensions 500 μm × 6 nm); placement of TEM grids is matched to film positions (*slits*) for the electrical measurements. *Right*: TEM micrographs of different nanostructural types (*dark*: metal; *light*: plasma polymer) (Ref. [42]; Copyright (2003) by the American Institute of Physics)

grating parameters lead to high efficient SPP excitation. The data showed significantly improved photon assisted tunneling (SPP photo-signal to background ratio) with an applied bias. Inside the metals, the SPP was assumed to decay partly into single particle excitations of electron which could drift to the oxide barrier and tunnel to the counter electrode. The photoresponse was thus determined by the generation of the electrons in metal films at the evanescent field of SPR and by the tunneling rates through the barrier. A mean free path of the hot electrons was estimated to be ~25 nm for the MOM junction. In an interesting report, detection of visible light by two dimensional (2D) Ag–Al_2O_3–Al based MOM tunnel junctions on glass with periodic array of bumps was reported [55]. The SPP at the periodic gratings decayed into single particle excitations, which had sufficient energy to tunnel through the oxide barrier. They obtained a rectification of the photoresponse at 476.9 nm due to the nonlinear *I–V* characteristic of the tunnel junction. In a fresh approach, a strong wavelength-dependent and reversible photoresponse was reported in a two-terminal device using a self-assembled ensemble of Au nanopeapodded silica nanowires under light illumination, whereas no photoresponse was observed for the plain silica nanowires (Fig. 1.8). The switching wavelength was found to match the SPR absorption leading to the generation of electrons in the evanescent field where the photogenerated electrons tunnel through

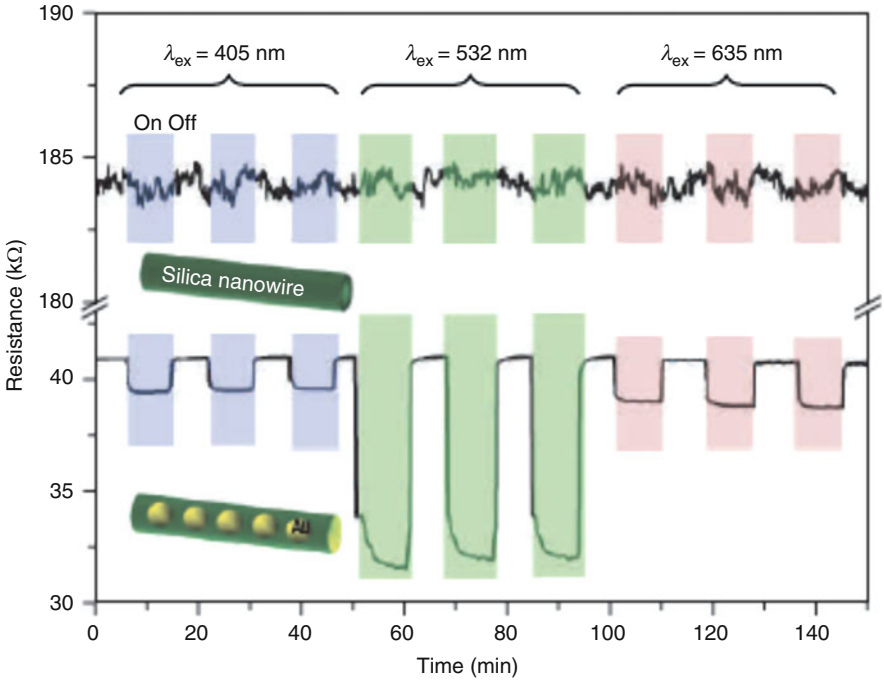

Fig. 1.8 Photoresponse measurements. The room-temperature resistance response as a function of time to light illumination for plain silica nanowires (*upper part*) and gold nanopeapodded silica nanowires (*lower part*). *Shaded* (*pink*, excitation wavelength $\lambda_{ex} = 635$ nm; *green*, $\lambda_{ex} = 532$ nm; *purple*, $\lambda_{ex} = 405$ nm) and *unshaded* regions mark the light-on and light-off periods, respectively (Ref. [33]; Copyright (2006) by the Nature Publication Group)

the oxide nanowires owing to the propagation of SPP. The propagating hot electron in the 1D nanoscale wave guide was observed to travel an inter-particle separation of 100 nm which was one order higher than that reported for MOM structures [43].

1.1.3 A Propagative Surface Plasmon for Electrical Transport

Albeit the origin of percolative pathway or tunneling of electrons at percolation threshold in explaining the observed photocurrent in noble metal-dielectric matrices, a plasmon coupling based propagation of SPP can always be envisaged in the understanding of optical switching. It is particularly important when pure quantum mechanical electron tunneling cannot be used for inter-particle separations above 10 nm. Thus the conception of SPP, where plasmonic coupling played a vital role in the formation of hot electron in evanescent field and its propagation, was the principal driving mechanism for the observed optical switching in noble

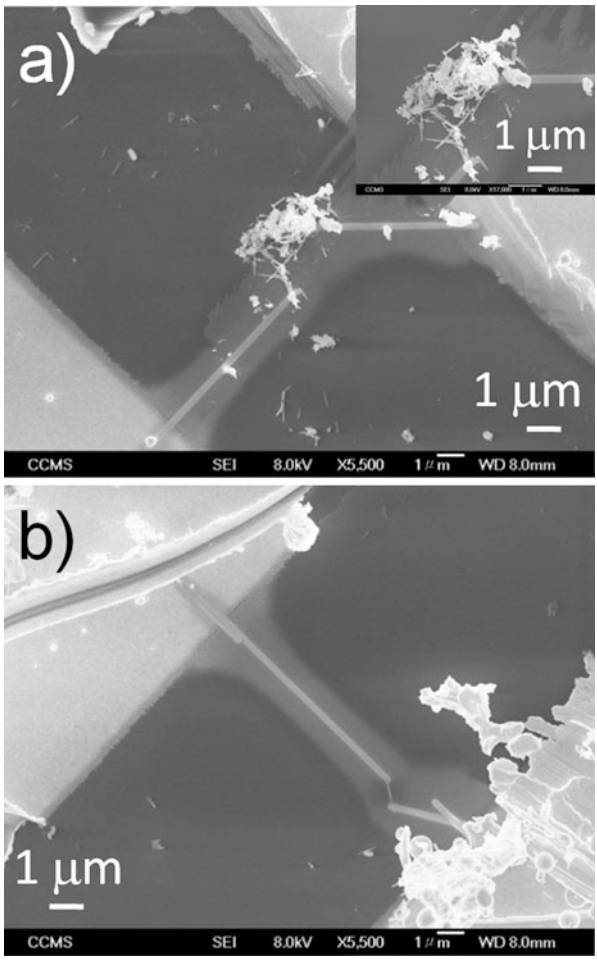

Fig. 1.9 Focused ion beam assisted Pt contact electrodes in (**a**) ensemble (**b**) single GaN nanowire system (Ref. [34]; Copyright (2014) by the Springer)

metal-dielectric matrices. The role of sub-band gap states, however was clearly understood for both percolative model considering 'site energy' correlated to Coulomb gap in the granular system [48, 50] and in tunneling model by definition with electron travelling through the potential barrier at the Fermi level.

In a recent study, optical switching for 1D Au–GaN nanowires and in a single nanowire (Fig. 1.9) was demonstrated [34] for sub-band gap (532 nm; GaN band gap at 365 nm) excitation with surface plasmon resonance peak of Au around 550 nm. Conduction process, responsible for the observed photoresponse (Fig. 1.10), was conceived as SPP assisted transport of electron with propagative resonating electromagnetic radiation coupled to Au nanoclusters generating the carriers (schematic in Fig. 1.11) [56]. Resistivity measurements in the single nanowire showed lowering of resistivity from the bulk value of 0.3 Ω-cm (measured at dark) to 0.05 Ω-cm for the 532 nm illumination as a measure of surface plasmon polariton assisted electrical conduction process [34].

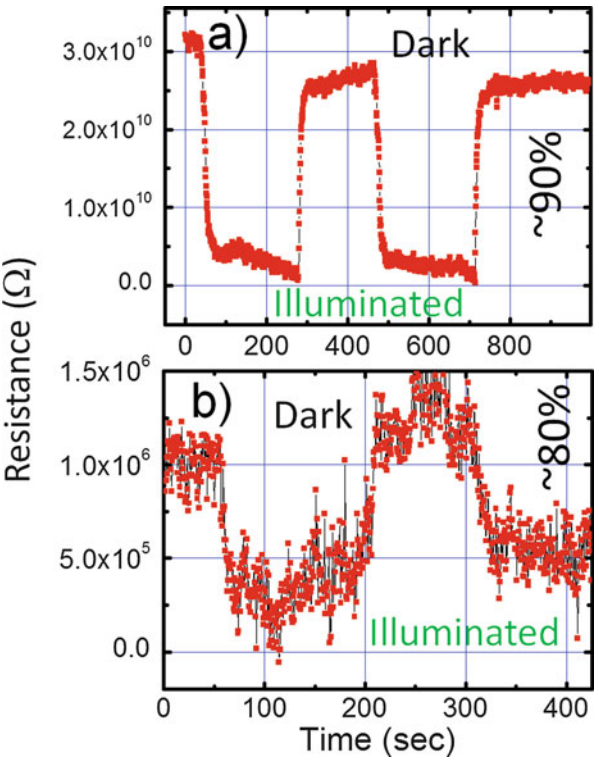

Fig. 1.10 Photoresponse in (**a**) ensemble (**b**) single GaN nanowire samples with periodical dark and 532 nm illumination conditions (Ref. [34]; Copyright (2014) by the Springer)

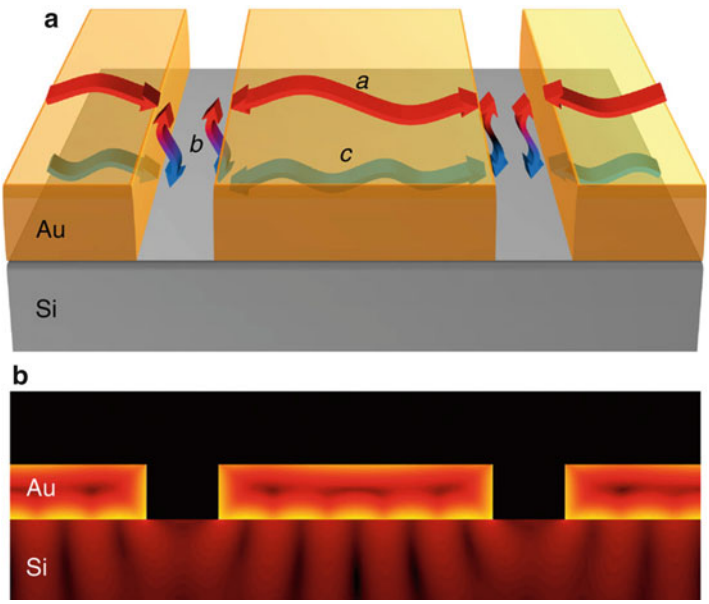

Fig. 1.11 Propagation of surface plasmons on gratings. (**a**) There are three forms of surface plasmon polaritons (SPPs) around each gold pitch: *a*, SPPs oscillating at the top surface of gratings; *b*, SPPs oscillating though the slits and; *c*, SPPs oscillating at the bottom surface of gratings at the Ti–Si Schottky interface. (**b**) Plasmonic heat absorption calculated by FDTD (shown with a logarithmic scale for clarity). Most of the hot electron generation occurs at the bottom surface of the *gold layer* (Ref. [56]; Copyright (2013) by the Nature Publication Group)

In a novel study, optical switching in the Au–Ag@SG system using 808 nm excitation was reported [40]. A change in current was almost twice for 808 nm excitation than that observed for the exposure with 532 nm (Fig. 1.12) indicating a possible role of TPA in the conduction process. The effect of TPA, unlike the conventional wisdom, was realized in its manifestation of doubling the photocurrent with the excitation wavelength of 808 nm as compared to 532 nm excitation where a single photon was involved in the SPR assisted photoresponse. In the sub-band gap picture, the SPP assisted generation of photocurrent does not occur across the band so a quadratic increase in the current cannot be expected. The photocurrent was because of the transport of conduction electrons belonging to Au–Ag system, so the role of TPA was limited to the plasmonic coupling the conduction electrons of Au–Ag system. In order to understand the possible role of competitive inter- and intraband transition in Au and Ag [57], FDTD calculations were analyzed showing very strong dipole coupling of Au–Ag@SG system for both 532 nm and 808 nm excitations for an inter-particle separation between Au and Ag nanoparticles of 2 nm (Fig. 1.13a). On the other hand, absence of electromagnetic coupling for 405 nm for the same system was noteworthy. The observation was correlated to the absence of interband contribution of Ag [56] to the electromagnetic light absorption process in the bimetallic system of Au and Ag. Dipole interaction between Au and Ag nanoparticles was reported active up to a gap of 4 nm for both 532 nm and 808 nm excitations (Fig. 1.13b). The role of larger layer being involved in the electrical conduction process at 808 nm (with low absorption

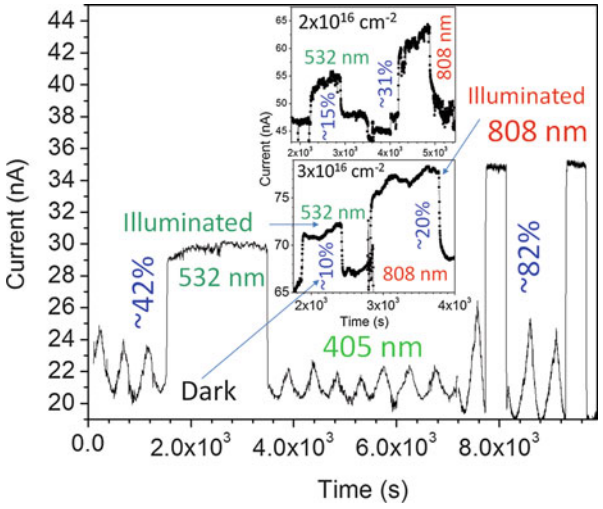

Fig. 1.12 Typical photoresponse of Au–Ag embedded in soda glass sample grown with Au^+ implantation at a fluence of 5×10^{16} ions.cm^{-2} with periodical dark and illumination to different laser wavelengths. Inset shows similar photoresponse of samples grown with Au^+ implantation at fluences of 2×10^{16} and 3×10^{16} ions.cm^{-2}. The studies show a double amount of change in current for 808 nm excitation than that observed for 532 nm exposure (Ref. [40]; Copyright (2015) by the American Institute of Physics)

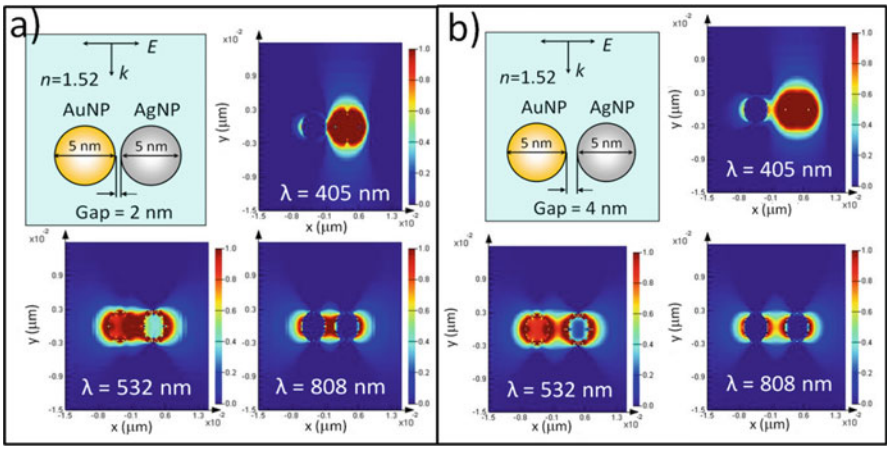

Fig. 1.13 Comparison of the electric field intensity enhancement contours for the interaction of electromagnetic radiation of different wavelengths with 5 nm Au and Ag nanoparticles separated by (**a**) 2 nm and (**b**) 4 nm in a medium with refractive index $n = 1.52$. Here k is the electromagnetic wave propagation vector, E is the electrical field vector and intensity bars indicate $|E|^2$ (Ref. [40]; Copyright (2015) by the American Institute of Physics)

of 808 nm in the bimetallic system) excitation and increasing the photocurrent to almost twice the value of that observed in for 532 nm exposure was ruled out in the presence of strong coupling of electromagnetic wave of both 532 and 808 nm in the Au–Ag system (Fig. 1.13). The observation suggested possibility of optical switching in noble bimetallic nanocluster system where long wavelength with higher skin depth can be used for the communication purpose [40].

References

1. MacDonald KF, Samson ZL, Stockman MI, Zheludev NI (2009) Ultrafast active plasmonics. Nat Photonics 3:55–58
2. Gramotnev DK, Bozhevolnyi SI (2010) Plasmonics beyond the diffraction limit. Nat Photonics 4:83–91
3. Bouhelier A, Bachelot R, Lerondel G, Kostcheev S, Royer P, Wiederrecht GP (2005) Surface plasmon characteristics of tunable photoluminescence in single gold nanorods. Phys Rev Lett 95:267405
4. Atwater HA, Polman A (2010) Plasmonics for improved photovoltaic devices. Nat Mater 9:205–213
5. Sonnichsen C, Reinhard BM, Liphardt J, Alivisatos AP (2005) A molecular ruler based on plasmon coupling of single gold and silver nanoparticles. Nat Biotechnol 23:741–745
6. Verhagen E, Spasenović M, Polman A, Kuipers L (2008) Nanowire plasmon excitation by adiabatic mode transformation. Phys Rev Lett 102:203904
7. Inouye H, Tanaka K, Tanahashi I, Hattori T, Nakatsuka H (2000) Ultrafast optical switching in silver nanoparticle system. Jpn J Appl Phys 39:5132–5133

8. Inouye H, Tanaka K, Kondo Y, Hirao K (1998) Femto second Optical Kerr effect in the gold nanoparticle system. Jpn J Appl Phys 37:L1520–L1522
9. Liao HB, Xiao RF, Fu JS, Yu P, Wong GKL, Sheng P (1997) Large third-order optical nonlinearity in Au:SiO_2 composite films near the percolation threshold. Appl Phys Lett 70:1–3
10. Haglund RF Jr, Yang L, Magruder RH III, Wittig JE, Becker K (1993) Picosecond nonlinear optical response of a Cu:silica nanocluster composite. Opt Lett 18:373–375
11. Maier SA, Kik PG, Atwater HA, Meltzer S, Harel E, Koel BE, Requicha AAG (2003) Local detection of electromagnetic energy transport below the diffraction limit in metal nanoparticle plasmon waveguides. Nat Mater 2:229–232
12. Andrew P, Barnes WL (2004) Energy transfer across a metal film mediated by surface plasmon polaritons. Science 306:1002–1005
13. Maier SA, Atwater HA (2005) Plasmonics: localization and guiding of electromagnetic energy in metal/dielectric structures. J Appl Phys 98:011101
14. Aihara T, Fukuhara M, Takeda A, Lim B, Futagawa M, Ishii Y, Sawada K, Fukuda M (2013) Monolithic integration of surface plasmon detector and metal-oxide-semiconductor field-effect transistors. IEEE Photonics J 5:6800609
15. Bozhevolni S, Volkov VS, Devaux E, Laluet JY, Ebbesen TW (2006) Channel plasmon subwavelength waveguide components including interferometers and ring resonators. Nature 440:508–511
16. Lezec HJ, Degiron A, Devaux E, Linke RA, Martin-Moreno L, Garcia-Vidal FJ, Ebbesen TW (2002) Beaming light from a subwavelength aperture. Science 297:820–822
17. Lewis A, Isaacson M, Harootunian A, Murray A (1984) Development of a 500 Å spatial resolution light microscope I. Light is efficiently transmitted through λ/16 diameter apertures. Ultramicroscopy 13:227–232
18. Pendry JB (2000) Negative refraction makes a perfect lens. Phys Rev Lett 85:3966–3969
19. Fang N, Lee H, Sun C, Zhang X (2005) Sub-diffraction-limited optical imaging with a silver superlens. Science 308:534–537
20. Hell SW (2007) Far-field optical nanoscopy. Science 316:1153–1158
21. Harootunian A, Betzig E, Isaacson MS, Lewis A (1986) Superresolution fluorescence near-field scanning optical microscopy (NSOM). Appl Phys Lett 49:674–676
22. Betzig E, Harootunian A, Lewis A, Isaacson M (1986) Near-field diffraction from a slit: implications for superresolution microscopy. Appl Optics 25:1890–1900
23. Kim S, Jin J, Kim Y-J, Park I-Y, Kim Y, Kim S-W (2008) High-harmonic generation by resonant plasmon field enhancement. Nature 453:757–760
24. McMahon MD, Lopez R, Haglund RF Jr, Ray EA, Bunton PH (2006) Second-harmonic generation from arrays of symmetric gold nanoparticles. Phys Rev B 73:041401
25. Bouhelier A, Beversluis M, Hartschuh A, Novotny L (2003) Near-field second-harmonic generation induced by local field enhancement. Phys Rev Lett 90:013903
26. Hubert C, Billot L, Adam P-M, Bachelot R, Royer P, Grand J, Gindre D, Dorkenoo KD, Fort A (2007) Surface plasmon spectralcharacteristics of second harmonic generation in gold nanorods. Appl Phys Lett 90:181105–181107
27. Nie SM, Emery SR (1997) Probing single molecules and single nanoparticles by surface-enhanced Raman scattering. Science 275:1102–1106
28. Bailoa E, Deckert V (2008) Tip-enhanced Raman scattering. Chem Soc Rev 37:921–930
29. Zhang R, Zhang Y, Dong ZC, Jiang S, Zhang C, Chen LG, Zhang L, Liao Y, Aizpurua J, Luo Y et al (2013) Chemical mapping of a single molecule by plasmon-enhanced Raman scattering. Nature 498:82–86
30. Brongersma ML, Hartman JW, Atwater HA (2000) Electromagnetic energy transfer and switching in nanoparticle chain arrays below the diffraction limit. Phys Rev B 62:R16356–R16359
31. Quinten M, Leitner A, Krenn JR, Aussenegg FR (1998) Electromagnetic energy transport via linear chains of silver nanoparticles. Opt Lett 23:1331–1333

32. Rycenga M, Cobley CM, Zeng J, Li W, Moran CH, Zhang Q, Qin D, Xia Y (2011) Controlling the synthesis and assembly of silver nanostructures for plasmonic applications. Chem Rev 111:3669–3712
33. Hu MS, Chen HL, Shen CH, Hong LS, Huang BR, Chen KH, Chen LC (2006) Photosensitive gold nanoparticle-embedded dielectric nanowires. Nat Mater 5:102–106
34. Dhara S, Lu C-Y, Chen K-H (2015) Plasmonic switching in Au functionalized GaN nanowires in the realm of surface plasmon polatriton propagation : a single nanowire switching device. Plasmonics 10:347–350
35. Kruss S, Srot V, van Aken PA, Spatz JP (2011) Au–Ag hybrid nanoparticle patterns of tunable size and density on glass and polymeric supports. Langmuir 28:1562–1568
36. Karthikeyan B (2012) Optical studies on thermally surface plasmon tuned Au, Ag and Au:Ag nanocomposite polymer films. Spectrochim Acta A Mol Biomol Spectrosc 96:456–460
37. Xu L, Tan LS, Hong MH (2011) Tuning of localized surface plasmon resonance of well-ordered Ag/Au bimetallic nanodot arrays by laser interference lithography and thermal annealing. Appl Optics 50:G74–G79
38. Tuan NA, Mizutani G (2009) Metal-interface second harmonic generation from pt/cu bimetallic nanowire arrays on NaCl(110) faceted templates. e-J Surf Sci Nanotech 7:831–835
39. Hoffbauer MA, McVeigh VJ (1990) Ultrafast optical probes of interface dynamics and structure. Proc SPIE Laser Photoionization Desorption Surf Anal Tech 1208:117
40. Dhara S, Lu C-Y, Magudapathy P, Huang Y-F, Tu W-S, Chen K-H (2014) Surface plasmon polariton assisted optical switching in noble bimetallic nanoparticle system. Appl Phys Lett 106:023101
41. Yang KY, Choi KC, Kang I-S, Ahn CW (2010) Surface plasmon resonance enhanced photoconductivity in Cu nanoparticle films. Opt Express 18:16379–16386
42. Kiesow A, Morris JE, Radehaus C, Heilmann A (2003) Switching behavior of plasma polymer films containing silver nanoparticles. J Appl Phys 94:6988–6990
43. Berthold K, Höpfel RA, Gornik E (1985) Surface plasmon polariton enhanced photoconductivity of tunnel junctions in the visible. Appl Phys Lett 46:626–628
44. Cohen RW, Cody GD, Coutts MD, Abeles B (1973) Optical properties of granular silver and gold films. Phys Rev B 8:3689–3701
45. Bruggeman DAG (1935) Berechnung verschiedener physikalischer Konstanten von heterogenen substanzen. Ann Phys (Leipzig) 24:636–679
46. Sheng P (1980) Theory for the dielectric function of granular composite media. Phys Rev Lett 45:60–63
47. Sheng P, Abeles B, Arie Y (1973) Hopping conductivity in granular metals. Phys Rev Lett 31:44–47
48. Simanek E (1980) The temperature dependence of the electrical resistivity of granular metals. Solid State Commun 40:1021–1023
49. Efros AL, Shklovskii BI (1975) Coulomb gap and low-temperature conductivity of disordered systems. J Phys C 8:L49–L51
50. Sheng P, Klafter J (1983) Hopping conductivity in granular disordered systems. Phys Rev B 27:2583–2586
51. Magudapathy P, Gangopadhyay P, Panigrahi BK, Nair KGM, Dhara S (2001) Electrical transport studies of Ag nano-clusters embedded in glass matrix. Phys B 299:142–146
52. Kreibig U, Vollmer M (1995) Optical properties of metal clusters. Springer, Berlin
53. Zhou P, You GJ, Li YG, Han T, Li J, Wang SY, Chen LY, Liu Y, Qian SX (2003) Linear and ultrafast nonlinear optical response of $Ag:Bi_2O_3$ composite films. Appl Phys Lett 83:3876–3878
54. del Coso R, Requejo-Isidro J, Solis J, Gonzalo J, Afonso CN (2005) Third order nonlinear optical susceptibility of $Cu:Al_2O_3$ nanocomposites: from spherical nanoparticles to the percolation threshold. J Appl Phys 95:2755–2762
55. Glass AM, Liao PF, Olson DH, Humphrey LM (1892) Optical metal-oxide tunnel detectors with microstructured electrodes. Opt Lett 7:575–577

56. Sobhani A, Knight MW, Wang Y, Zheng B, King NS, Brown LV, Fang Z, Nordlander P, Halas NJ (2013) Narrowband photodetection in the near-infrared with a plasmon-induced hot electron device. Nat Commun 4:1–6
57. Dhara S, Kesavamoorthy R, Magudapathy P, Premila M, Panigrahi BK, Nair KGM, Wu CT, Chen KH (2003) Quasiquenching size effects in gold nanoclusters embedded in silica matrix. Chem Phys Lett 370:254–260

Chapter 2
Modeling and Interpretation of Hybridization in Coupled Plasmonic Systems

Saïd Bakhti, Nathalie Destouches, and Alexandre V. Tishchenko

Abstract The coupled mode formalism is introduced to provide a phenomenological understanding of the coupling effects in finite systems of particles. Within this approach, a metal nanoparticle can be viewed as an optical resonator and the formation of hybrid modes, resulting from the coupling between particles, can be anticipated. An efficient numerical algorithm is proposed to extract the characteristics (complex poles and amplitudes) of each resonance of the system.

The spectral behavior of the eigen modes of a single metal sphere is analyzed. The redshift and broadening of the different modes with the increase of the particle size and the local refractive index are characterized. Optimal conditions can be found to maximize the particle absorption as well as the near-field enhancement. Sub-radiant and super-radiant hybrid modes of a dimer are identified from the extinction spectrum of each particle. These hybrid modes have different energetic behavior depending on the inter-particle distance, and can then be compared to bounding (attractive) and anti-bounding (repulsive) states. The near-field enhancement resulting from the hybrid mode excitation is maximized by optimizing the dimer geometry and the surrounding refractive index.

The hybrid modes in a quadrumer are identified. For small particles with a reduced coupling via scattering, the system exhibits an anti-crossing behavior of the hybrid modes typical for weakly coupled resonators. When the particles are sufficiently large to induce a strong coupling in the system, the extinction spectrum of the quadrumer present Fano-like resonances, i.e. resonances with an asymmetric line shape. The hybrid modes at the origin of these particular resonances are identified as sub- and super-radiant modes of the system. The sharp Fano-like resonance has a high figure of merit, making such system promising for sensing applications.

Keywords Plasmon resonances • Coupled mode approach • Metal nanoparticles • Hybrid modes • Fano resonances

S. Bakhti • N. Destouches • A.V. Tishchenko (✉)
CNRS, UMR5516, Hubert Curien Laboratory, Saint-Etienne F-42000, France
e-mail: tishchen@univ-st-etienne.fr

C.D. Geddes (ed.), *Reviews in Plasmonics 2015*,
DOI 10.1007/978-3-319-24606-2_2

2.1 Introduction

Plasmon resonances induced by the electromagnetic excitation of metal nanoparticles are generally associated with the presence of resonance bands in the spectral response of these nanoparticles [1], and lead to an increase in the local electromagnetic field at resonance wavelengths [2]. Each band corresponding to a particular mode of resonance is characterized by its spectral position and width. These spectral characteristics are strongly dependent on the geometry of the particles as well as on their environment. Changes in the resonance bands result in a red shift of the resonance position as well as in a broadening of the bands when the size of the particle or the local refractive index increases.

In general, the optical response of metal nanoparticles is largely dominated by bands of plasmon resonances. As part of a study of the spectral evolution of these different bands based on certain geometric and environmental parameters, it may be more convenient to deal only with resonance parameters (position and width) rather than considering the whole optical spectra. Different methods allow for retrieving these parameters; they are based on Mie theory for spheres [3], the eigenvalues of surface integrals [4], or the hybridization theory for more complex systems [5, 6]. We propose here to develop a method to extract precisely the resonance parameters from the total optical response of a system of particles based on the T-matrix method and its generalization to multi-particle systems [7, 8]. The main objective of this development is to provide an efficient and flexible numerical tool for the characterization of plasmon resonances together with a phenomenological approach to interpret their physical behavior [9–11].

We first introduce the coupled mode model applied to the phenomenological description of the plasmon resonance amplitudes resulting from an external excitation, allowing a treatment of metal nanoparticles as optical resonators. This model is applied to a single resonance mode and extended to a pair of coupled modes, providing a set of phenomenological parameters including losses, coupling with excitation and mutual coupling coefficients. This approach anticipates the formation of hybrid modes as resulting from the coupling between two plasmon modes. The coupled mode model is applied to the complex valued extinction coefficient of the individual particles, defined as an extension of the classical extinction cross-section. This coefficient, having the same phase than the dipolar moment of the particles, appears as a convenient parameter to identify the nature of the hybrid modes in a coupled system. The solutions of the coupled mode equations being in the form of a singular function of the pulsation, we propose an efficient numerical algorithm to extract the characteristics (complex poles and amplitudes) of each resonance of the system from the rigorous computation of complex valued extinction coefficients. All phenomenological parameters describing the coupling between particles can be deduced from these characteristics.

Within this theoretical framework, we first analyze the spectral behavior of the eigenmodes of a single silver sphere. The redshift and broadening of the different modes with the increase of the particle size and the local refractive index are characterized and optimal conditions are found to maximize the particle absorption as well as the near-field enhancement. The case of a silver dimer is then studied,

where sub-radiant and super-radiant hybrid modes are identified from the extinction spectrum of each particle. These hybrid modes have different energetic behaviors depending on the inter-particle distance, and can then be compared to bounding (attractive) and anti-bounding (repulsive) states. Local field enhancement resulting from hybrid mode excitation can be maximized by optimizing the dimer geometry and the surrounding refractive index. Our method is finally applied to silver quadrumers, where hybrid modes exhibit an anti-crossing behavior in the case of weakly coupled small particles. For larger particles, their strong coupling induces the appearance of a Fano-like resonance in extinction spectra. The hybrid modes at the origin of this sharp asymmetric resonance line shape are identified and their behavior is analyzed, showing their potential for sensing applications.

2.2 Coupled Mode Model Applied to Interacting Plasmon Modes

We determine in this section an equation governing the coupled plasmon mode amplitudes, with a few phenomenological parameters characterizing the coupling behavior in simple plasmonic systems. The proposed formalism is well known in the classical coupled mode theory [12] and can be applied to more complex geometries.

A single plasmon mode can be described by a first order differential equation giving the time variations of the mode amplitude $a(t)$ when excited by an incident wave with electric field $f_0(t)$

$$\frac{da(t)}{dt} = -j\mathrm{Re}\{\omega_p\}a(t) - \frac{1}{\tau}a(t) + \kappa f_0(t) \tag{2.1}$$

where τ is the time decay of the plasmon (representing the total losses in the resonant system including absorption as well as re-radiation attributed to scattering), κ is the coupling coefficient and ω_p is the complex resonant angular frequency of the plasmon mode. The real part of ω_p corresponds to the resonance position and the imaginary part to its half width at half maximum (HWHM). When both the incident radiation and the plasmon amplitude oscillate at angular frequency ω, they can be expressed in terms of their modulation amplitudes $\widetilde{f}_0(t)$ and $\tilde{a}(t)$ respectively

$$\begin{cases} f_0(t) = \widetilde{f}_0(t)\exp\{-j\omega t\} \\ a(t) = \tilde{a}(t)\exp\{-j\omega t\} \end{cases} \tag{2.2}$$

Substituting these expressions into Eq. (2.1) and fixing condition $\widetilde{f}_0(t) = 1$ which corresponds to a plane wave with unit amplitude we get the following particular solution of Eq. (2.1) in steady state

$$\widetilde{a}(\omega) = \frac{j\kappa}{\omega - \mathrm{Re}\{\omega_p\} + \frac{j}{\tau}} \tag{2.3}$$

Final modulation amplitude $\tilde{a}$ depends on angular frequency ω only and the obtained expression can be written in a very simple form as:

$$\widetilde{a}(\omega) = \frac{a_p}{\omega - \omega_p} \tag{2.4}$$

where the coupling coefficient is related with amplitude as $a_p = j\kappa$, and the time decay corresponds to the imaginary part of the complex pulsation $\mathrm{Im}\{\omega_p\} = -1/\tau$. The coupling coefficient quantifies the coupling between the incident excitation and the plasmon mode. Its amplitude provides the coupling strength and its phase corresponds to the oscillator phase at resonance relative to the excitation.

In the case of close particles, plasmon resonances strongly interact, resulting in the formation of hybrid modes in the system. To generalize the phenomenological description to coupled systems, consider first two interacting plasmon modes. One can write two coupled-mode equations on the basis of Eq. (2.1). Two modes with amplitudes $a_1(t)$ and $a_2(t)$ and complex angular eigen frequencies ω_1 and ω_2 are coupled to the incident radiation with coupling coefficients κ_1 and κ_2. Phenomenological equations managing these modes can be written in the following form:

$$\begin{cases} \dfrac{da_1(t)}{dt} = -j\mathrm{Re}\{\omega_1\}a_1(t) + \mathrm{Im}\{\omega_1\}a_1(t) + \kappa_1 f_0(t) + \kappa_{12}a_2(t) \\ \dfrac{da_2(t)}{dt} = -j\mathrm{Re}\{\omega_2\}a_2(t) + \mathrm{Im}\{\omega_2\}a_2(t) + \kappa_2 f_0(t) + \kappa_{21}a_1(t) \end{cases} \tag{2.5}$$

where κ_{12} and κ_{21} are the coupling coefficients between the two modes. The temporal amplitudes of the modes can be expressed in terms of their temporal envelope similarly to the case of a single mode:

$$\begin{cases} a_1(t) = \widetilde{a}_1(t)\exp(-j\omega t) \\ a_2(t) = \widetilde{a}_2(t)\exp(-j\omega t) \end{cases} \tag{2.6}$$

Substituting expressions (2.6) into Eq. (2.5), we get rid of the fast oscillating term $\exp(-j\omega t)$. The particular solution of the coupled mode equations is found in steady state, when $\widetilde{f}_0(t) = 1$:

$$\begin{cases} \widetilde{a}_1(\omega) = \dfrac{a_1^+}{\omega - \omega^+} + \dfrac{a_1^-}{\omega - \omega^-} \\ \widetilde{a}_2(\omega) = \dfrac{a_2^+}{\omega - \omega^+} + \dfrac{a_2^-}{\omega - \omega^-} \end{cases} \tag{2.7}$$

The solutions appear as a linear superposition of two singular functions, showing that the coupling between the plasmon modes results in the formation of two hybrid modes with complex resonance angular frequencies ω^+ and ω^- distinct from the original modal angular frequencies. The values of the phenomenological parameters a_1^-, a_1^+, a_2^-, a_2^+, ω^+ and ω^- of these hybrid modes can be found by fitting the